Journal of Catalysis 280 (2011) 168–177

Contents lists available at ScienceDirect

Journal of Catalysis

journal homepage: www.elsevier.com/locate/jcat

Effect of the CH_3OH/H_2O ratio on the mechanism of the gas-phase photocatalytic reforming of methanol on noble metal-modified TiO_2

Gian Luca Chiarello [a], Davide Ferri [b], Elena Selli [a,*]

[a] Dipartimento di Chimica Fisica ed Elettrochimica, CIMAINA and ISTM-CNR, Università degli Studi di Milano, Via Golgi 19, I-20133 Milano, Italy
[b] Empa – Swiss Federal Laboratories for Materials Science and Technology, Lab. for Solid State Chemistry and Catalysis, Ueberlandstrasse 129, CH-8600 Duebendorf, Switzerland

ARTICLE INFO

Article history:
Received 5 October 2010
Revised 16 March 2011
Accepted 18 March 2011
Available online 22 April 2011

Keywords:
Photo-steam reforming of methanol
Photocatalytic H_2 production
Pt/TiO_2
Au/TiO_2
Reaction mechanism
H_2O/D_2O isotopic exchange

ABSTRACT

The photocatalytic reforming of methanol was investigated kinetically under steady conditions as a function of the methanol-to-water partial pressure ratio in the gas mixture fed to the photoreactor. Similar results were obtained with two TiO_2-based photocatalysts, one containing platinum nanoparticles and prepared by flame spray pyrolysis and the other prepared by the deposition of preformed Au nanoparticles on P25 TiO_2. Methanol oxidation proceeds on the photocatalyst surface up to CO_2 through the formation of formaldehyde and formic acid as intermediate species. The steady-state formaldehyde, formic acid, and carbon dioxide production rates, plotted *vs*. the methanol molar fraction in the aqueous solution generating the gaseous reaction mixture, were successfully fitted on the basis of a reaction scheme, in which each elementary oxidation step occurs through either an indirect $^{\cdot}OH$ radical-mediated path, or a hole-mediated direct path, or a water-assisted path, when oxidation occurs on titania surface sites far from noble metal nanoparticles. H_2O/D_2O isotopic-exchange experiments allow a clear distinction between the direct and the indirect oxidation paths and fully support the proposed reaction scheme.

1. Introduction

The photocatalytic production of hydrogen from water over semiconductor metal oxides, in particular TiO_2, has received renewed, extensive attention in the last decade for its potential application in the field of solar energy harvesting, conversion, and storage [1–3].

The photocatalytic splitting of pure water is generally characterized by relatively low hydrogen production rates, mainly due to the fast recombination of the electron–hole pairs photoproduced on the surface of semiconductor photocatalysts and to the occurrence of back reactions on the irradiated photocatalyst surface. The separation of the photoproduced charge carriers can be greatly increased if noble metal nanoparticles, able to trap conduction band electrons [4,5], are deposited on the semiconductor surface, as well as in the presence of organic species, *e.g.,* methanol, able to act as hole scavenger more efficiently than water [6] and undergo faster and irreversible oxidation. This may proceed either through (i) the direct interaction of organics with the free or trapped holes in the semiconductor's valence band (VB) [7–9] or (ii) *via* the attack of the $^{\cdot}OH$ radicals produced by the reaction of valence band holes with surface hydroxyl groups or adsorbed water [9–11]. These reaction paths may occur in parallel and can hardly be distinguished one from the other [12,13].

Recently, the photocatalytic production of hydrogen from methanol–water vapors (*i.e.,* the photocatalytic reforming reaction of methanol) has been investigated systematically by us over a platinum-containing TiO_2 photocatalyst [5]. Methanol was found to undergo oxidation up to CO_2 through the formation of formaldehyde and formic acid as intermediate species; carbon monoxide, methane, methyl formate, dimethyl ether, and acetaldehyde were also identified as side products. The study has now been performed also with a gold-containing TiO_2 photocatalyst, prepared by the deposition of preformed Au nanoparticles on commercial P25 TiO_2, to collect kinetic data with another noble metal-containing photocatalyst prepared by a different route, thus exhibiting different structural and surface features. Final aim of our investigation was to ascertain how the formation rate of both intermediates (formaldehyde and formic acid) and final main reaction products (hydrogen and carbon dioxide) depend on the methanol/water molar ratio in the reactant mixture. In particular, we aimed at understanding the origin of the observed decrease in the carbon dioxide production rate with increasing the methanol molar fraction in comparison with the bell-shaped trends observed for formaldehyde and formic acid production rates. The results of our thorough kinetic analyses have been interpreted on the basis of a proposed reaction sequence occurring on the photocatalyst surface and the desorption of the intermediate species, by a Langmuir–Hinshelwood-type kinetic model [14–20], able to satisfactorily fit all the experimental data obtained with the two photocatalysts at different methanol/water molar ratios. Steady-state isotopic exchange

* Corresponding author. Fax: +39 02 503 14300.
E-mail address: elena.selli@unimi.it (E. Selli).

0021-9517/$ - see front matter © 2011 Elsevier Inc. All rights reserved.
doi:10.1016/j.jcat.2011.03.013

experiments, allowing a clear distinction between the direct and the hydroxyl radical–mediated oxidation paths, have also been performed to support the proposed reaction scheme.

2. Experimental

2.1. Preparation and characterization of photocatalysts

All chemicals, of high purity grade, were purchased from Aldrich and used as received. The TiO_2 photocatalyst containing 0.5 wt.% of platinum, denoted 0.5%Pt/TiO_2, was synthesized by flame spray pyrolysis (FP) in a single step [21], starting from a xylene–acetonitrile solution containing titanium(IV)-isopropoxide and platinum acetyl acetonate [5]. The gold-containing photocatalyst was prepared by deposition of preformed, surfactant-stabilized Au nanoparticles on commercial Degussa P25 TiO_2, according to the reverse micelle method [22]. The TiO_2 powder, previously ultrasonically dispersed in water, was added under vigorous stirring to an Au colloidal suspension, obtained by adding $NaBH_4$ (4:1 $NaBH_4$ to Au molar ratio) to a *n*-dodecyl-trimethylammonium chloride aqueous solution containing chloroauric acid (40:1 surfactant-to-Au molar ratio). The precipitated colored powder was separated, thoroughly washed with water, centrifuged, and dried in oven at 70 °C overnight [5]. This photocatalyst contained 1.0 wt.% gold and was labeled 1%Au/TiO_2.

The two photocatalysts were characterized as already described [5]. Their BET specific surface area was measured by N_2 adsorption/desorption at 77 K in a Micromeritics ASAP 2010 apparatus. UV–vis diffuse reflectance analysis was performed by means of a Perkin-Elmer Lambda 35 apparatus, equipped with a Labsphere RSA-PE-20 integration sphere. High angular annular dark field–scanning transmission electron microscopy (HAADF-STEM) was carried out on a JEOL FS2200-FEG instrument, operated at 200 kV. X-ray diffraction data were collected with a Philips PW3020 powder diffractometer, and quantitative crystal phase analysis was performed by the Rietveld refinement method, using the "Quanto" software.

2.2. Photocatalytic tests

The rates of hydrogen, carbon dioxide, carbon monoxide, formaldehyde, and formic acid production in the photo-steam reforming reaction of methanol were determined using the equipment [23], procedure, and experimental conditions described elsewhere [5]. Repeated runs carried out under identical conditions ensured a reproducibility of rate results within 5%. Briefly, the photoreactor consisted in a 50-mm-diameter, 2-mm-thick, cylindrical Plexiglas cell frontally closed with an illuminated Pyrex glass optical window and was inserted in a closed stainless steel system, previously purged with nitrogen, where the gas phase was recirculated at constant rate (40 mL min^{-1}). The inert gas was saturated with methanol–water vapors by continuously bubbling it into a methanol–water solution kept at 30 °C and then fed to the photoreactor. The water-to-methanol partial pressure ratio was varied by changing the methanol molar fraction x in the liquid solution, in the range $0.0045 \leqslant x \leqslant 1$. The irradiation source was an iron halogenide mercury arc lamp, equipped with a shutter. During irradiation, the gas-phase composition was determined on-line at the photoreactor exit, by gas-chromatographic (GC) analysis, employing an Agilent 6890 N apparatus [5]. H_2, CO_2, and CO accumulated at constant rate in the recirculating gas phase, whereas the gas-phase concentration of the formaldehyde and formic acid intermediates at the exit of the photoreactor remained practically constant, because they were trapped and accumulated in the liquid solution. The final concentration of formaldehyde and formic acid in the liquid solution was determined by GC analysis and by ion chromatography (IC) with conductivity detection, employing a Metrohm 761 instrument [5], respectively.

2.3. Isotopic exchange photocatalytic tests

The H_2O/D_2O isotopic exchange photocatalytic tests were performed using the same photoreactor and light source. The gas-phase composition at the exit of the photoreactor was monitored on-line by quadrupolar mass spectrometry (QMS) employing an Omnistar Pfeiffer Vacuum GSD 301O2 apparatus connected through a heated (150 °C) stainless steel capillary tube. Because of the sampling mode of the QMS instrument, these experiments could not be performed in the recirculation mode. Thus, the photocatalyst bed was continuously fed with H_2O/CH_3OH or D_2O/CH_3OH vapors, obtained by bubbling flowing argon (40 mL min^{-1}) in a methanol–water or methanol–D_2O liquid solution thermostated at 30 °C. Three different CH_3OH molar fractions (x = 0.0045, 0.10, and 0.64) were considered. The experiments were started by flowing the reactants through the photoreactor in the dark for 5 min, followed by three consecutive, ca. 30-min-long irradiation cycles, spaced by 5 min in the dark, while continuously flowing the reactant gas mixture.

3. Results and discussion

3.1. Characterization of photocatalysts

FP-0.5%Pt/TiO_2 consisted of micro-aggregates of single-crystal nanospheres, 10–25 nm in diameter, as revealed by HAADF-STEM analysis (Fig. 1), containing 53% anatase and 47% rutile, with a specific surface area of 70 m^2 g^{-1}. The 1%Au/TiO_2 sample had the typical structural features of P25 TiO_2, consisting of widely condensed, irregularly shaped, ca. 20 nm in size crystalline aggregates (Fig. 1),

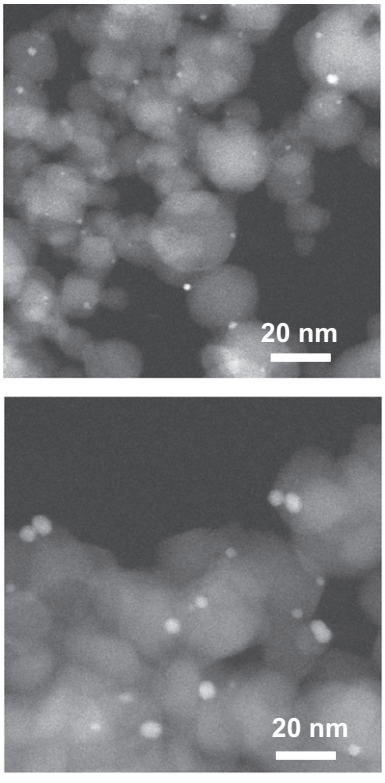

Fig. 1. STEM-HAADF images of FP-0.5%Pt/TiO_2 (upper image) and 1%Au/TiO_2 (lower image). Noble metal nanoparticles appear as bright dots on the titania support due to their higher *Z*-contrast.

with a 48 $m^2 g^{-1}$ specific surface area and a mixed crystal phase composition of ca. 80% anatase and 20% rutile. The low-temperature method adopted for noble metal deposition did not alter the bulk properties of TiO_2 [5].

The images reported in Fig. 1 evidence well-dispersed, ca. 1.5- to 3-nm-sized Pt nanoparticles in the FP-made sample, appearing as bright dots due to the different Z-contrast of the noble metal with respect to the titania support. Slightly larger, *i.e.*, 3- to 8-nm-sized, gold nanoparticles are present in the 1%Au/TiO_2 sample, together with a few larger ones, up to 20 nm in size. Thus, FP confirmed to be an effective method for the direct synthesis of relatively high surface area photocatalytic materials containing small and well-dispersed noble metal nanoparticles [23,24].

Both materials exhibited a UV–vis absorption threshold below 400 nm [5]. The gold-containing oxide also displayed the typical plasmon resonance band of gold nanoparticles (<20 nm), centered at 550 nm, *i.e.*, red shifted compared with the plasmon resonance band of pure gold (520 nm), due to alteration of the electronic configuration of gold because of its interaction with the titania support. With a broad absorption in the visible region, 0.5%Pt/TiO_2 appeared as a light-gray powder [5].

3.2. Photocatalytic activity

During irradiation, the amount of both hydrogen and carbon dioxide increased linearly in the recirculated gas phase [5]. Thus, their production rates, r_{H_2} and r_{CO_2}, were determined as the slope of the straight lines interpolating their gas-phase concentration *vs.* time plots. By contrast, the amount of formaldehyde and formic acid in the gas mixture outcoming from the photoreactor rapidly attained values that remained practically constant during irradiation. In fact, these oxidation intermediates were continuously produced at almost constant rate in the photoreactor, as a consequence of adsorbed methanol oxidation, followed by desorption, and continuously trapped in the liquid solution by the subsequent bubbling through it. No appreciable increase in the formaldehyde content in the gas phase outcoming from the photoreactor was detected during the runs [5], because its very small increase in the gas phase, based on vapor–liquid equilibrium, was negligible with respect to the formaldehyde amount produced in the photoreactor. The average production rates r_{H_2CO} and r_{HCOOH} were therefore estimated from the final formaldehyde and formic acid amounts in the solution at the end of the runs, divided by the overall irradiation time, assuming constant production rates.

Fig. 2 reports the rate of H_2 production, r_{H_2}, and the selectivity in hydrogen production to CO_2 and to formic acid, defined as $S_{CO_2} = 3r_{CO_2}/r_{H_2} \times 100$ and $S_{HCOOH} = 2r_{HCOOH}/r_{H_2} \times 100$, respectively [5], determined with both FP-0.5%Pt/TiO_2 and 1%Au/TiO_2 as a function of the molar fraction x of methanol in the liquid phase. Very similar trends were obtained when employing the two noble metal-modified photocatalysts under identical irradiation conditions, demonstrating a common behavior, almost independent of the nature and loading of the noble metal, and also of the photocatalyst preparation method.

In particular, both r_{H_2} and S_{HCOOH} exhibit an asymmetric bell-shaped trend with a maximum located at $0.2 < x < 0.65$. Furthermore, at low x values, r_{H_2} is lower than at high x values. On the other hand, the rate of CO_2 production r_{CO_2}, and also S_{CO_2}, display a decay trend with increasing x, the r_{CO_2} maximum being attained at high water-to-methanol molar ratios. Furthermore, as the partial pressure of methanol increases, S_{CO_2} decreases and formaldehyde becomes the main methanol oxidation product. These results clearly show the crucial role of water in guaranteeing the attainment of complete oxidation in the vapor-phase photoreforming of methanol under anaerobic conditions.

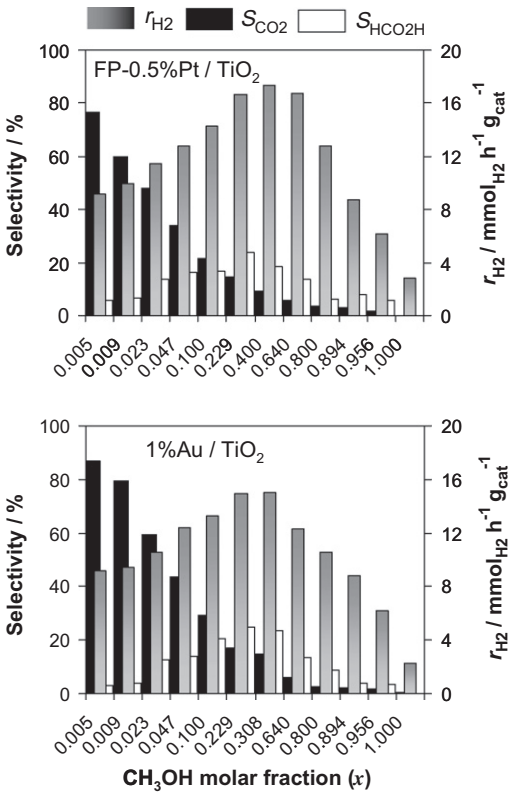

Fig. 2. Hydrogen production rate (r_{H_2}) and selectivity to CO_2 (S_{CO_2}) and to formic acid (S_{HCOOH}) as a function of the methanol molar fraction x in the liquid solution in equilibrium with the gas mixture fed to the photoreactor.

3.3. Reaction mechanism

The photocatalytic reforming of methanol occurs on the semiconductor surface after light absorption and band gap excitation [25]. Consequently, the following elementary steps should be considered in the photocatalytic reaction mechanism:

(i) Light absorption and generation of $e^-_{CB} - h^+_{VB}$ pairs:

$$TiO_2 + h\nu \rightarrow e^-_{CB} + h^+_{VB} \quad (1)$$

The rate of this initial step is $I_a\Phi$, I_a being the amount of photons absorbed per unit time and Φ the quantum efficiency of step (1) [25].

(ii) The adsorption of electron acceptor and donor species, EA and ED, on the photocatalyst cathodic and anodic adsorption surface sites, respectively: $EA_g \leftrightarrows EA_{ads}$ and $ED_g \leftrightarrows ED_{ads}$.

(iii) The reaction of photoproduced charge carriers e^-_{CB} and h^+_{VB} with acceptor or donor species, respectively, adsorbed on the photocatalyst surface: $EA_{ads} + e^-_{CB} \rightarrow P_{1,ads}$ and $ED_{ads} + h^+_{VB} \rightarrow P_{2,ads}$, in competition with the very fast e^-_{CB} and h^+_{VB} recombination, releasing heat Q:

$$e^-_{CB} + h^+_{VB} \xrightarrow{k_{recomb}} TiO_2 + Q \quad (2)$$

(iv) The desorption of products (or intermediate species in a multistep mechanism) from the photocatalyst surface: $P_{1,ads} \leftrightarrows P_{1,g}$ and $P_{2,ads} \leftrightarrows P_{2,g}$.

In the case of the photocatalytic steam reforming of methanol under anaerobic conditions on TiO_2 modified by noble metal nanoparticles' deposition, oxidation occurs on the titania surface and

both methanol and water can act as ED species [25], whereas photopromoted electrons accumulate in noble metal nanoparticles, acting as photocathode, where protons, the EA species, undergo reduction to H_2.

The sequence of photoinduced oxidation reactions occurring on the photocatalyst surface under steady-state conditions is schematically represented in Fig. 3. Methanol and water are known to adsorb competitively on the oxide surface, both molecularly or dissociatively, with the formation of surface hydroxyl and methoxy groups [26–34]. Adsorbed methanol is then oxidized up to CO_2 on the photocatalyst surface, through formaldehyde and formic acid formation, as intermediate species. Under steady-state conditions, the surface concentration of the intermediates is constant and a competition is established at each step between further oxidation and desorption of the adsorbed intermediate species. In particular, the higher is the desorption rate with respect to the oxidation rate, the higher is the accumulation rate of that intermediate in the gas phase and consequently the lower is the selectivity to CO_2.

Under the adopted experimental conditions, the composition of the gas mixture fed to the photoreactor did not vary substantially during the runs and it contained negligible amounts of the formaldehyde and formic acid intermediates, which were efficiently trapped by the liquid solution, where they accumulated, though their content always remained extremely low [5]. Moreover, the sum of the rates of H_2CO, HCOOH and CO_2 formation was equal to the overall rate of methanol conversion, at least for low methanol/water ratios, *i.e.,* when negligible amounts of species containing two carbon atoms were produced [5]. Hence, under steady-state conditions, although methanol oxidation to CO_2 occurred through a series of consecutive surface reactions, the reaction system can also be envisaged as a set of three parallel reactions yielding the above-mentioned main three products (Fig. 3).

More in detail, the following series of elementary steps are able to account for the photocatalytic anaerobic oxidation of methanol and the detected intermediate species:

$$H_2O_g \underset{k_{-w}}{\overset{k_w}{\leftrightarrows}} H_2O_{ads} \tag{3}$$

$$CH_3OH_g \underset{k_{-m}}{\overset{k_m}{\leftrightarrows}} CH_3OH_{ads} \tag{4}$$

$$H_2O_{ads} + h^+_{VB} \xrightarrow{k_1} {\cdot}OH_{ads} + H^+_{ads} \tag{5}$$

$$CH_3OH_{ads} + {\cdot}OH_{ads}\left(\text{or } h^+_{VB}\right) \xrightarrow{k_2} CH_3O^{\cdot}_{ads} + H_2O\left(\text{or } H^+_{ads}\right) \tag{6}$$

$$CH_3O^{\cdot}_{ads} + {\cdot}OH_{ads}\left(\text{or } h^+_{VB}\right) \xrightarrow{k'_2} H_2CO_{ads} + H_2O\left(\text{or } H^+_{ads}\right) \tag{7}$$

$$H_2CO_{ads} \xrightarrow{k_{des,H_2CO}} H_2CO_g \tag{8}$$

$$H_2CO_{ads} + {\cdot}OH_{ads}\left(\text{or } h^+_{VB}\right) \xrightarrow{k_3} HCO^{\cdot}_{ads} + H_2O\left(\text{or } H^+_{ads}\right) \tag{9}$$

$$HCO^{\cdot}_{ads} + {\cdot}OH_{ads} \xrightarrow{k'_3} HCOOH_{ads} \tag{10}$$

$$HCOOH_{ads} \xrightarrow{k_{des,HCOOH}} HCOOH_g \tag{11}$$

$$HCOOH_{ads} + {\cdot}OH_{ads}\left(\text{or } h^+_{VB}\right) \xrightarrow{k_4} {\cdot}COOH_{ads} + H_2O\left(\text{or } H^+_{ads}\right) \tag{12}$$

$${\cdot}COOH_{ads} + {\cdot}OH_{ads}\left(\text{or } h^+_{VB}\right) \xrightarrow{k'_4} CO_{2,ads} + H_2O\left(\text{or } H^+_{ads}\right) \tag{13}$$

$$CO_{2,ads} \xrightarrow{k_{des,CO_2}} CO_{2,g} \tag{14}$$

$$2H^+_{ads} + 2e^-_{CB} \xrightarrow{k_{red}} H_2 \tag{15}$$

In this reaction sequence, each oxidation step may proceed on the photocatalyst surface either by the direct interaction of the adsorbed organic species with valence band holes, h^+_{VB}, or by an indirect path involving hydroxyl radical attack [8–12]. Any ·OH radical-mediated path implies, first of all, water adsorption, which reacts with valence band holes, producing protons and reactive ·OH radicals adsorbed on the photocatalyst surface. Each hole-mediated oxidation step produces adsorbed H^+, which are also produced in the water oxidation step yielding ·OH radicals, reaction (5). Photocatalytic hydrogen production results from reaction (15), *i.e.,* from the reduction of adsorbed protons by conduction band electrons, accumulated on noble metal nanoparticles under irradiation. When the photocatalytic reforming of methanol is carried out in contact with the gas phase, a very crucial point is the diffusion of the so-produced protons over the titania surface toward the reduction sites, a point that will be better enlightened later on.

Note that reaction (10) cannot proceed through a direct, hole-mediated path, but can only proceed through hydroxyl radical attack, because an extra oxygen atom is needed to transform H_2CO into HCOOH, which can only be provided indirectly by water, through a hydroxyl radical.

3.4. Rate expressions

Under steady-state conditions, the concentration of all species adsorbed on the photocatalyst surface is constant. Therefore, by indicating with r_j the rate of the jth step:

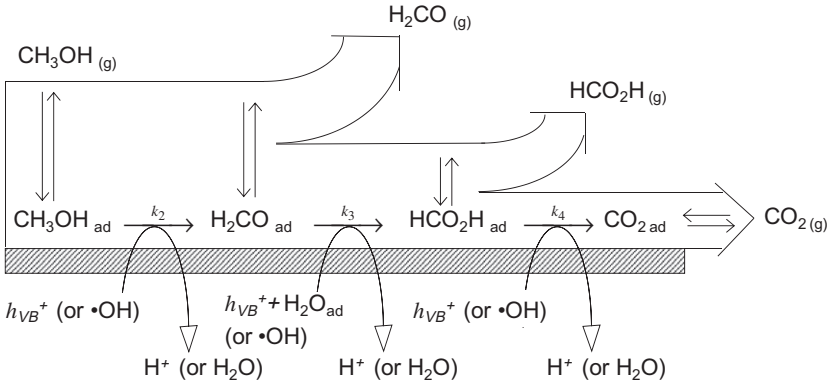

Fig. 3. Reaction scheme of the photocatalytic vapor phase oxidation of methanol on the TiO_2 surface under steady-state conditions.

$$\frac{d[CH_3O^{\cdot}_{ads}]}{dt} = r_2 - r'_2 = 0 \quad (16)$$

$$\frac{d[H_2CO_{ads}]}{dt} = r'_2 - r_3 - r_{des,H_2CO} = 0 \quad (17)$$

$$\frac{d[CHO^{\cdot}_{ads}]}{dt} = r_3 - r'_3 = 0 \quad (18)$$

$$\frac{d[HCOOH_{ads}]}{dt} = r'_3 - r_4 - r_{des,HCOOH} = 0 \quad (19)$$

$$\frac{d[HCOO^{\cdot}_{ads}]}{dt} = r_4 - r'_4 = 0 \quad (20)$$

$$\frac{d[CO_{2,ads}]}{dt} = r'_4 - r_{des,CO_2} = 0 \quad (21)$$

where $r_{des,i}$ are the desorption rates of the ith species detected in the gas phase at the exit of the photoreactor, which coincide with their overall accumulation rates in the liquid solution (in the case of formaldehyde and formic acid) or in the recirculating gas (carbon dioxide). Of course, from Eqs. (16)–(21), it follows:

$$r_{des,H_2CO} + r_{des,HCOOH} + r_{des,CO_2} = r_2 \quad (22)$$

which is nothing but the mass balance condition in terms of r_2, the rate of methanol oxidation. Furthermore, from Eqs. (16)–(21), it also follows that the measured H_2CO, HCOOH, and CO_2 production rates are equal to:

$$r_{des,H_2CO} = r'_2 - r_3 = r_2 - r_3 \quad (23)$$

$$r_{des,HCOOH} = r'_3 - r_4 = r_3 - r_4 \quad (24)$$

$$r_{des,CO_2} = r'_4 = r_4 \quad (25)$$

According to the proposed reaction scheme, the rate of each oxidation step occurring on the photocatalyst surface is the sum of the rates of the direct and of the hydroxyl radical-mediated paths, apart in the case of r'_3, as mentioned before. For instance, for $j = 2$ the following rate expression can be written for methanol oxidation:

$$r_2 = k_2^{OH}\theta_{OH}\theta_{CH_3OH} + k_2^h[h^+_{VB}]\theta_{CH_3OH} \quad (26)$$

where, in general, k_j^{OH} and k_j^h are the rate constants of the hydroxyl radical-mediated and hole-mediated paths, respectively, for the jth elementary oxidation step on the photocatalyst surface, $[h^+_{VB}]$ is the surface concentration of valence band holes under irradiation and θ_i is the fraction of surface sites covered by the ith species adsorbed on the photocatalyst surface. However, surface coverages $\theta_{H_2CO}, \theta_{HCOOH}$ and θ_{CO_2} cannot be evaluated from gas-phase measurements, and consequently equations similar to Eq. (26) for $j = 3$ and 4 are not useful in the development of a reaction kinetic model.

On the other hand, from Eq. (22) it follows that, under steady-state conditions, the reaction system in the gas phase can be envisaged as methanol undergoing three parallel reactions, yielding the three products H_2CO, HCOOH, and CO_2. Thus, the rate constants k_2^{OH} and k_2^h appearing in Eq. (26), relative to methanol oxidation, can be taken as the sum of the k_i^{OH} and k_i^h formation rate constants of the three products, according to the indirect and the hole-mediated paths, respectively:

$$k_2^{OH} = k^{OH}_{H_2CO} + k^{OH}_{HCOOH} + k^{OH}_{CO_2} = \sum k_i^{OH} \quad (27)$$

$$k_2^h = k^h_{H_2CO} + k^h_{HCOOH} + k^h_{CO_2} = \sum k_i^h \quad (28)$$

so that the formation rate of the ith product can in general be expressed as:

$$r_i = k_i^{OH}\theta_{OH}\theta_{CH_3OH} + k_i^h[h^+_{VB}]\theta_{CH_3OH} \quad (29)$$

i.e., the overall rate of formation of each product is the sum of the rate contribution of the direct and the indirect path, expressed in terms of methanol surface coverage.

The surface coverage of ·OH radicals under steady-state conditions, θ_{OH}, can be obtained from Eqs. (5)–(13), as follows:

$$\frac{d[OH_{ads}]}{dt} = k_1[h^+_{VB}]\theta_{H_2O} - \theta_{OH}\left(k_2^{OH}\theta_{CH_3OH} + \sum k_j^{OH}\theta_i\right) = 0 \quad (30)$$

$$\theta_{OH} = \frac{k_1[h^+_{VB}]\theta_{H_2O}}{k_2^{OH}\theta_{CH_3OH} + \sum k_j^{OH}\theta_i} \quad (31)$$

The concentration of valence band holes $[h^+_{VB}]$ under steady-state conditions can be obtained by taking into account Eqs. (1), (2), and (5)–(13):

$$\frac{d[h^+_{VB}]}{dt} = I_a\Phi - k_{recomb}[h^+_{VB}][e^-_{CB}] - [h^+_{VB}]\left(k_1\theta_{H_2O} + \sum k_j^h\theta_i\right) = 0 \quad (32)$$

All measurements in the present study were carried out under continuous irradiation, *i.e.*, under conditions that do not allow a distinction between "free" and "trapped" holes and electrons photogenerated upon semiconductor excitation [8]. Eq. (32) can be simplified by considering that charge recombination in semiconductors is expected to be much faster than any electron transfer reaction [8]. Consequently, $I_a\Phi \cong k_{recomb}[h^+_{VB}][e^-_{CB}]$. Furthermore, if one assumes that the steady-state concentration of photopromoted electrons equals that of photoproduced holes, *i.e.*, $[h^+_{VB}] \approx [e^-_{CB}]$ for charge balance, then:

$$[h^+_{VB}] = \sqrt{\frac{I_a\Phi}{k_{recomb}}} \quad (33)$$

Thus, under the above-mentioned assumptions, the concentration of valence band holes depends only on the irradiation conditions (I_a) and on the photocatalyst intrinsic properties (Φ and k_{recomb}). The extent of charge separation increases in the presence of noble metal nanoparticles deposited on the semiconductor surface [8]. In fact, these are able to efficiently capture conduction band electrons, with the consequent decrease in k_{recomb} and increase in charge carriers steady-state concentration, with more efficient interface electron transfer paths and higher rates of overall photocatalytic reactions.

By substituting Eqs. (31) and (33) into Eq. (29), and by recalling that $[h^+_{VB}]$ and C_S are constant under the adopted experimental conditions (the same photocatalyst amount and light intensity were always used), the general expression for the formation rates of the ith product is obtained:

$$r_i = \sqrt{\frac{I_a\Phi}{k_{recomb}}}\left\{\frac{k_i^{OH}k_1\theta_{H_2O}\theta_{CH_3OH}}{k_2^{OH}\theta_{CH_3OH} + \sum k_j^{OH}\theta_i} + k_i^h\theta_{CH_3OH}\right\} \quad (34)$$

If the surface coverages θ_i appearing in Eq. (34) are expressed according to the Langmuir adsorption isotherm, *i.e.*, $\theta_i = K_ip_i/(1 + \sum_i K_ip_i)$, K_i and p_i being the adsorption equilibrium constant under irradiation and the partial pressure of the ith component, one finally obtains:

$$r_i = \frac{k_i'^{OH}K_{H_2O}p_{H_2O}K_{CH_3OH}p_{CH_3OH}}{\left(k_2^{OH}K_{CH_3OH}p_{CH_3OH} + \sum k_j^{OH}K_ip_i\right)\left(1 + K_{H_2O}p_{H_2O} + K_{CH_3OH}p_{CH_3OH} + \sum K_ip_i\right)} + \frac{k_i'^hK_{CH_3OH}p_{CH_3OH}}{\left(1 + K_{H_2O}p_{H_2O} + K_{CH_3OH}p_{CH_3OH} + \sum K_ip_i\right)} \quad (35)$$

where $k_i'^{OH}$ and $k_i'^h$ are constant, $K_{H_2O}(= k_w/k_{-w}$ see Eq. (3)), $K_{CH_3OH}(= k_m/k_{-m}$ see Eq. (4)), and K_i are the adsorption

equilibrium constants of H_2O, of CH_3OH and of the intermediate species on the illuminated photocatalyst surface; p_{H_2O}, p_{CH_3OH} and p_i are the partial pressures of H_2O, CH_3OH and of the ith species in the reaction gas mixture. These latter, however, have negligible values with respect to water and methanol vapor pressure, under the adopted experimental conditions. Thus, the $\sum k_j K_i p_i$ and $\sum K_i p_i$ terms can be neglected in Eq. (35) and the $K_{CH_3OH} p_{CH_3OH}$ term appearing at the nominator and at the denominator of the first right-hand term of Eq. (35) can be eliminated. Furthermore, by taking into account the non-ideal behavior of the liquid solution, one may express $p_{CH_3OH} = \gamma_{CH_3OH} x p^\circ_{CH_3OH}$ and $p_{H_2O} = \gamma_{H_2O}(1-x) p^\circ_{H_2O}$, x being the methanol molar fraction in the liquid solution, γ_{H_2O} and γ_{CH_3OH} the activity coefficients of H_2O and CH_3OH for that solution composition, $p^\circ_{H_2O}$ and $p^\circ_{CH_3OH}$ the water and methanol vapor pressure, respectively. The activity coefficients at the different x values have been calculated using the van Laar equation [35], with the activity coefficients at infinite dilution $\gamma^\infty_{CH_3OH}$ and $\gamma^\infty_{H_2O}$ equal to 1.95 and 1.59, respectively.

By introducing the above partial pressure expressions into Eq. (35), one finally obtains:

$$r_i = k_i'^{OH} \frac{\gamma_{H_2O} A(1-x)}{1 + \gamma_{H_2O} A + x\left(\gamma_{CH_3OH} B - \gamma_{H_2O} A\right)} + k_i'^{h} \times \frac{\gamma_{CH_3OH} B x}{1 + \gamma_{H_2O} A + x\left(\gamma_{CH_3OH} B - \gamma_{H_2O} A\right)} \quad (36)$$

where $A = K_{H_2O} p^\circ_{H_2O}$, $B = K_{CH_3OH} p^\circ_{CH_3OH}$, $k_i'^{OH} = \frac{k_i^{OH} k_1}{k_2}\sqrt{\frac{I_a \Phi}{k_{recomb}}}$ and $k_i'^{h} = k_i^h \sqrt{\frac{I_a \Phi}{k_{recomb}}}$. Eq. (36) is an approximation of Eq. (35), which correctly predicts a reaction rate equal to zero for $x = 0$ (*i.e.*, for $p_{CH_3OH} = 0$). The contribution of the $^{\cdot}OH$ radical-mediated path (first term of the right-hand side of Eqs. (35) and (36)) rapidly increases with increasing x, with a maximum located at a very low x value, followed by a decay trend with increasing x, which is faster, the higher is B with respect to A.

The plot of the CO_2 production rate *vs.* x (Fig. 4) follows indeed this type of behavior. Fig. 4 also displays the fitting of the experimental CO_2 production rate data (dotted lines) according to $^{\cdot}OH$ radical-mediated oxidation path (first term of the right-hand side of Eq. (36)). By comparing the experimental results with the

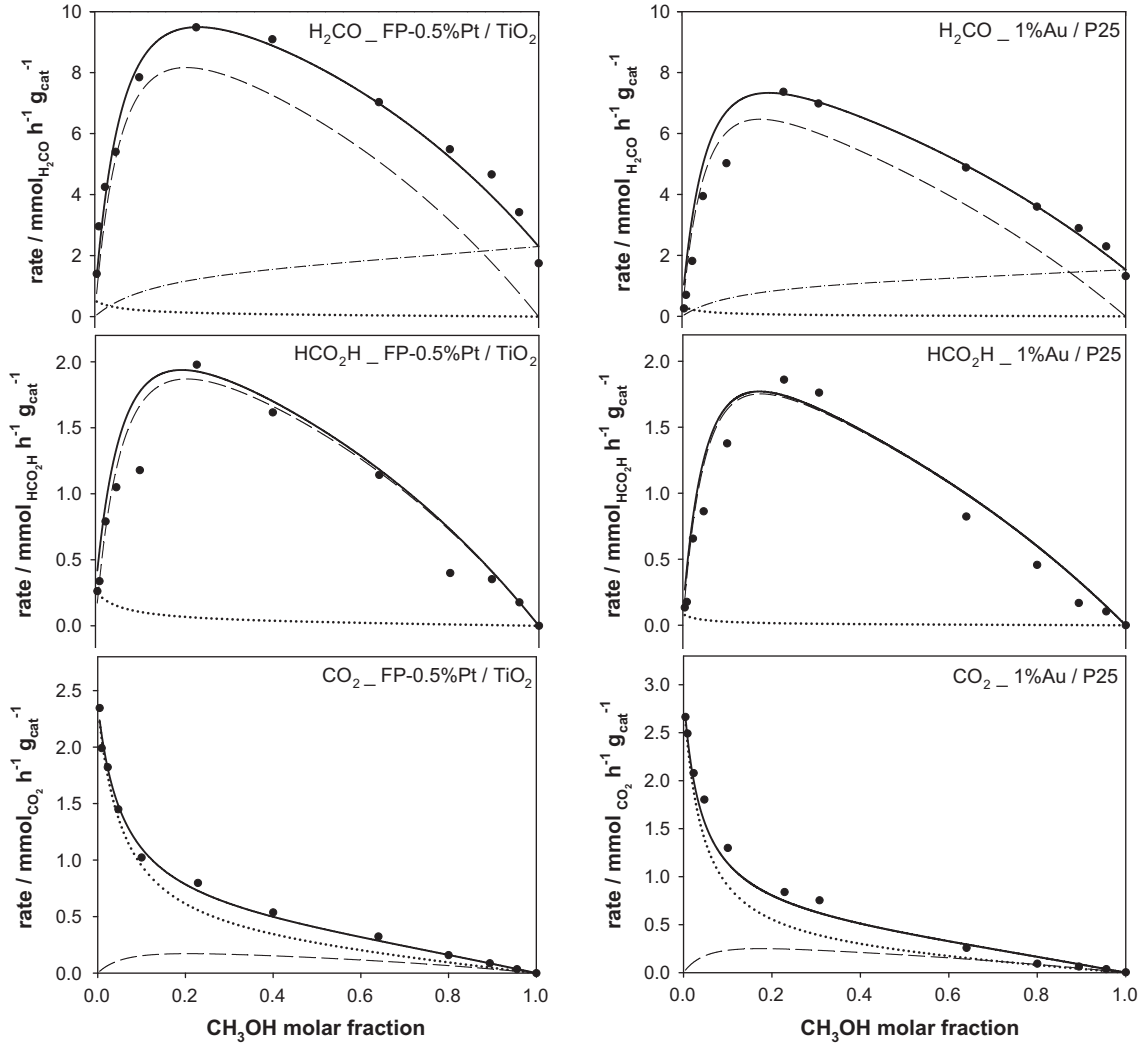

Fig. 4. Rates of formaldehyde, formic acid, and carbon dioxide production measured with FP-0.5%Pt/TiO_2 (left panels) and 1%Au/TiO_2 (right panels) at different methanol molar fraction x in the liquid phase in equilibrium with the gas mixture fed to the photoreactor. The fits according to the sum of Eqs. (36) and (38) for H_2CO and the first term only of Eqs. (36) and (38) for HCOOH and CO_2 (solid line) are also reported. Contributions of the oxidation paths: indirect path (dotted line); direct path (dashed dotted lines), and water-assisted path (dashed line).

calculated curve one may conclude, from a qualitative point of view, that CO_2 is preferentially photoproduced *via* this reaction path at high water partial pressure (low x values), whereas a significant variation in the reaction path occurs with increasing x, the experimental CO_2 production rate becoming higher than that predicted on the basis of this reaction path only.

The second term of the right-hand side of Eq. (36) accounts for the contribution of the hole-mediated oxidation path to the overall reaction rate. It follows a typical saturation, Langmuir-type behavior with increasing x, correctly predicting no reaction for $x = 0$, with a contribution to the overall rate tending to the maximum value $B/(1 + B)$ for $x = 1$. However, formaldehyde was the only product detected when the reactant was pure methanol (see Fig. 2), whereas the overall formation rate of both formic acid and carbon dioxide dropped to zero for $x = 1$, as expected from the stoichiometry of the reaction sequence, as already mentioned. This means that $k^h_{HCOOH} = k^h_{CO_2} = 0$ in Eq. (28) and consequently $k^h_2 = k^h_{H_2CO}$.

3.5. The water-assisted path

Eq. (36) alone is thus inadequate to describe the bell-shaped curves of formaldehyde and formic acid production rate *vs.* x (Fig. 4). Another reaction path must be at work, in which water does not act simply as a source of $^{\cdot}OH$ radicals. Indeed, water, besides being a reactant providing an oxygen atom in the oxidation step from formaldehyde to formic acid, may play another important role, *i.e.,* as a diffusion medium for protons produced at each oxidation step on the titania surface, toward the noble metal. Protons can be transferred over the TiO_2 surface by means of stable pairs of hydroxyl groups interacting with adsorbed water molecules [30,34]. In this respect, reaction sites located at the titania–noble metal interface should be distinguished from the reaction sites of the titania surface far from the noble metal. Methanol adsorbed on the first type of sites can directly transfer a proton to the noble metal during the oxidation step to formaldehyde through the reaction with a valence band hole. By contrast, the hole-mediated oxidation of methanol adsorbed on the second type of sites must be regarded as a "water-assisted" path, implying transfer of protons through neighbor hydroxyl groups up to the noble metal particles.

Thus, the rate-determining step of any hole-mediated oxidation path occurring on the photocatalyst surface sites far from the noble nanoparticles is expected to involve water molecules, which are able to stabilize the so-formed protons and transfer them to the noble metal, where they undergo reduction. The rate of this water-assisted path $r_{i,wa}$ depends on the surface concentration of both water and methanol, besides on that of photoproduced holes, according to the following rate expression:

$$r_{i,wa} = k_{i,wa}\left[h^+_{VB}\right]\theta_{CH_3OH}\theta_{H_2O} \tag{37}$$

By rearranging this equation according to a procedure analogous to that previously detailed to obtain Eq. (36), one finally gets:

$$r_{i,wa} = k'_{i,wa}\frac{\gamma_{H_2O}A\gamma_{CH_3OH}Bx(1-x)}{\left[1+\gamma_{H_2O}A + x(\gamma_{CH_3OH}B - \gamma_{H_2O}A)\right]^2} \tag{38}$$

where $k'_{i,wa} = k_{i,wa}\sqrt{\frac{I_a\Phi}{k_{recomb}}}$ is the observed rate constant of the water-assisted path. Eq. (38) describes a bell-shaped curve as a function of x, with $r_{i,wa} = 0$ for $x = 1$ or $x = 0$ and a maximum, determined by setting to zero the first derivative of the right-hand side of Eq. (38), presumably located at $x_{max} < 0.5$, because we expect $B > A$, $p^\circ_{CH_3OH}$ being ca. five times higher than $p^\circ_{H_2O}$.

3.6. Fitting the experimental rate results

The rates of formaldehyde, formic acid, and carbon dioxide production (r_{H_2CO}, r_{HCOOH} and r_{CO_2}) determined with the two photocatalysts at different methanol molar fractions x were fitted by considering the coexistence of the indirect $^{\cdot}OH$-mediated, the direct, and the water-assisted path described above, *i.e.,* according to an analytical function obtained by summing Eqs. (36) and (38). However, only in the case of formaldehyde production the direct path was relevant in the fitting of r_{H_2CO} data, as already outlined, whereas r_{HCOOH} and r_{CO_2} data were fitted by an analytical function obtained by summing the first term only of Eq. (36) with Eq. (38).

The photocatalyst surface is expected to bear sites with different distributions of adsorption strength. Hence, the A and B parameters in Eqs. (36) and (38) are related to the average adsorption constants of water and methanol, respectively. The same values of the A and B parameters were imposed in the fitting routine of r_{H_2CO}, r_{HCOOH} and r_{CO_2}. However, for a better fitting of r_{CO_2} results, the B parameter appearing in the first term of Eq. (36) was refined independently of that appearing in Eq. (38), as discussed below. The results of the fitting procedure, presented in Fig. 4, exhibit a good agreement with the measured rate values. Fig. 4 reports the overall predicted production rates as solid lines, together with their deconvolution into the contribution of the indirect (dotted lines), direct (dashed dotted line), and water-assisted (dashed lines) paths.

The B value obtained for the indirect path was higher than that obtained for the other paths (70 *vs.* 23 for FP-0.5%Pt/TiO_2 and 85 *vs.* 22 for 1%Au/TiO_2), suggesting that the adsorbed organic species involved in the indirect oxidation path are more strongly adsorbed on the photocatalyst surface. This also explains the high r_{CO_2} value at low x. Indeed, based on the reaction scheme proposed here, the more strongly the reacting species adsorb on the photocatalyst surface, the more the reaction shifts toward CO_2 formation, because the rate of further oxidation of the intermediate species on the titania surface is higher than their desorption rate. Also, aromatic alcohols have been recently reported to interact with the TiO_2 surface in different ways, resulting in either partial selective oxidation to aldehydes or mineralization [36,37].

The $^{\cdot}OH$-radical-mediated path prevails only for very low x values, *i.e.,* for low methanol partial pressure and thus relatively low surface coverage. Methanol is known to be a more effective hole scavenger than water [6]; thus, the indirect oxidation path prevails only at very low methanol coverage, when the probability of water reaction with valence band holes is high. Moreover, at low coverage, the highest energy adsorption sites are the first to be occupied. With increasing x, the indirect oxidation path rapidly falls down and the direct, water-assisted path becomes predominant for $x > 0.18$.

Slightly different fitting parameters are reported in Table 1 for the two photocatalysts, indicating that the same photocatalytic reaction paths are at work on their surface under irradiation. The small differences in the values of each parameter obtained from kinetic data collected when employing the two photocatalysts reflect small differences in their properties consequent to the different preparation method, *i.e.,* different exposed faces, surface hydroxyl concentration, size, and distribution of noble metal nanoparticles, without any substantial change in the mechanism to be attributed to the substitution of gold for platinum nanoparticles on the TiO_2 surface.

3.7. Isotopic exchange experiments

Isotopic exchange of H_2O with heavy water (D_2O) allows one to distinguish between the direct and the indirect oxidation paths.

Table 1
Refined values of parameters A, B and k/mmol h^{-1} g_{cat}^{-1} of Eqs. (36) and (38), obtained by fitting the r_{H_2CO}, r_{HCOOH} and r_{CO_2} *vs.* x data recorded with FP-0.5%Pt/TiO_2 and 1%Au/TiO_2 (see Fig. 4).

Photocatalyst	Oxidation path	r_{H_2CO}			r_{HCOOH}			r_{CO_2}		
		k	A	B	k	A	B	k	A	B
FP-0.5%Pt/TiO_2	Indirect	0.64	7.5	70	0.29	7.5	70	2.7	7.5	70
	Water-assisted	38	7.5	23	8.7	7.5	23	0.82	7.5	23
	Direct	2.4	–	23	–	–	–	–	–	–
1%Au/TiO_2	Indirect	0.42	6.2	85	0.11	6.2	85	3.4	6.2	85
	Water-assisted	31	6.2	22	8.4	6.2	22	1.2	6.2	22
	Direct	1.6	–	22	–	–	–	–	–	–

Indeed, when the reactants are D_2O and CH_3OH and only the indirect reaction path is supposed to be at work, the following reaction scheme can be written:

$$D_2O + h_{VB}^+ \rightarrow {}^{\cdot}OD + D^+ \quad (39)$$

$$CH_3OH + 2{}^{\cdot}OD \rightarrow CH_2O + 2HDO \quad (40)$$

$$CH_2OH + 2{}^{\cdot}OD \rightarrow HCOOD + HDO \quad (41)$$

$$HCOOD + 2{}^{\cdot}OD \rightarrow CO_2 + HDO + D_2O \quad (42)$$

$$2D^+ + 2e_{CB}^- \rightarrow D_2 \quad (43)$$

Therefore, if only an indirect reaction path were at work, only dideuterium molecules (D_2) are expected to be produced according to Eqs. (39) and (43), together with four HDO molecules, see Eqs. (40)–(42), for each methanol molecule undergoing full oxidation to CO_2.

By contrast, if methanol oxidation occurred only through the direct path, the reaction scheme would be:

$$CH_3OH + 2h_{VB}^+ \rightarrow CH_2O + 2H^+ \quad (44)$$

$$CH_2O + D_2O + 2h_{VB}^+ \rightarrow HCOOD + D^+ + H^+ \quad (45)$$

$$HCOOD + 2h_{VB}^+ \rightarrow CO_2 + D^+ + H^+ \quad (46)$$

$$2D^+ + 4H^+ + 6e_{CB}^- \rightarrow zHD + (1-z)D_2 + (2-z)H_2 \quad (\text{with } 0 \le z \le 1) \quad (47)$$

Therefore, if the reaction proceeds through a direct oxidation path, no HDO is expected to be produced and, based on the reaction stoichiometry, the photoproduced gas would contain 33.3% of D-atoms and 66.7% of H-atoms, statistically distributed in the form of HD, D_2 and H_2, Eq. (47). However, in the water-assisted direct oxidation path implying H^+ diffusion on the photocatalyst surface (through D_2O in the case of the deuterated system), some isotopic exchange between H^+ and D^+ can be expected to occur, before a noble metal nanoparticle is reached, which implies an increase of the D content of the photoproduced gas mixture.

By taking into account that the reaction in fact proceeds through the three paths simultaneously, HDO is expected to be produced, together with some HD, D_2 and H_2, with a D-atom content in the outcoming gas greater than 33.3%, depending on the relative weight of the three reaction paths.

Typical results of QMS analysis in the photocatalytic experiments performed with FP-0.5%Pt/TiO_2 fed with H_2O/CH_3OH/Ar or D_2O/CH_3OH/Ar at x = 0.0045 are reported in Fig. 5. In the first case (Fig. 5, upper panel), H_2, CO_2, HCOOH, and traces of CO formed under irradiation, with no variation of the signals at m/Z 3 (HD), 4 (D_2), and 19 (HDO) when irradiation began. By contrast, when the D_2O/CH_3OH/Ar mixture was fed to the reactor, HD, D_2, and HDO were produced under irradiation. The same variation of the

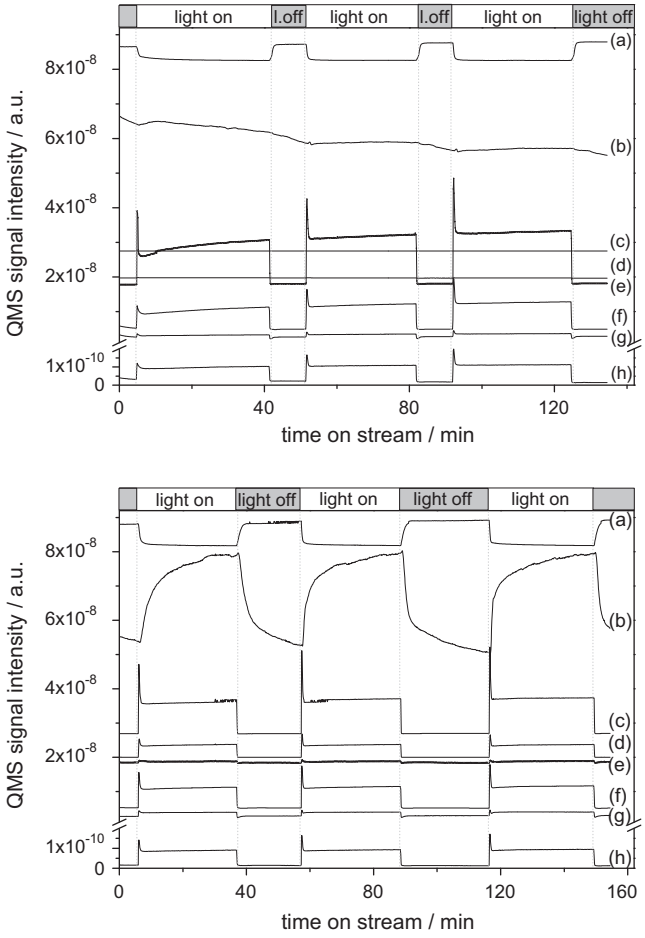

Fig. 5. Typical QMS signal intensity *vs.* time-on-stream, recorded during the photocatalytic experiment with FP-0.5%Pt/TiO_2 in flowing H_2O/CH_3OH/Ar (top) and D_2O/CH_3OH/Ar (bottom), with x = 0.045, in three consecutive irradiation cycles. The traces correspond to the following m/Z signals: (a) 31, corresponding to the $^+CH_2$ = OH fragment of methanol; (b) 19, HDO; (c) 4, D_2; (d) 3, HD; (e) 2, H_2; (f) 44, CO_2; (g) 28, CO; (h) 46, HCOOH.

m/Z = 44 signal, corresponding to CO_2, was observed in the two cases, confirming that the overall photoactivity was not affected by the substitution of D_2O for H_2O. Steady-state irradiation conditions were attained within the first 20 min, and two consecutive irradiation cycles led to the same variation of QMS signals. An intense peak of the QMS signals was observed when the shutter was opened (light on), followed by a plateau, as a consequence of the fact that interface electron transfer involving species adsorbed on the surface is much faster than the adsorption of reactants. (The photocatalyst surface is saturated in the dark.) The percent amount of H_2, HD, and D_2 at the photoreactor exit was calculated from the

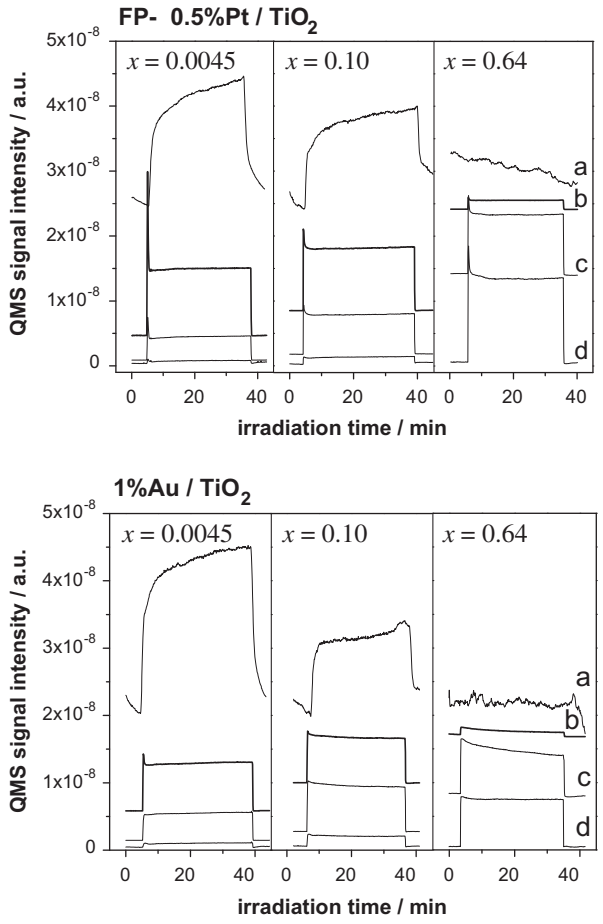

Fig. 6. QMS signals intensity *vs.* time during the third illumination cycle, recorded with FP-0.5%Pt/TiO_2 and 1%Au/TiO_2 when fed with D_2O/CH_3OH vapors in Ar, for three different methanol molar fractions (x = 0.0045, 0.10, and 0.64). The traces correspond to the following m/Z values: (a) 19, HDO; (b) 4, D_2; (c) 3, HD and (d) 2, H_2.

Table 2
Percent amounts of D_2, HD, and H_2 in the gas stream at the exit of the photoreactor measured by QMS in H_2O/D_2O isotopic exchange experiments with the two tested photocatalysts at different values of the methanol molar fraction x in the CH_3OH/D_2O solution.

	x	D_2 (%)	HD (%)	H_2 (%)	H (%)	D (%)
FP-0.5%Pt/TiO_2	0.0045	72	27	1	14	86
	0.10	57	36	7	25	75
	0.64	7	39	54	74	26
1% Au/TiO_2	0.0045	60	35	5	23	77
	0.10	46	45	9	32	68
	0.64	6	44	50	72	28

variation of the corresponding QMS signal after the beginning of irradiation.

The m/Z signals of H_2, HD, D_2, and HDO recorded with the two photocatalysts at the third illumination cycle carried out with three different methanol molar fractions (x = 0.0045, 0.10 and 0.64) are reported in Fig. 6, and their percent amounts calculated from QMS signals are collected in Table 2. The percent deuterium content was always higher than expected from the reaction stoichiometry and significantly decreased with increasing x. This result confirms, in line with the fitting results shown in Fig. 4, that at low x (x = 0.0045 and 0.10) the indirect, ·OH-radical-mediated oxidation path prevails, D_2 being the main product, accompanied by HDO formation, whereas at high x (*i.e.,* at x = 0.64) the direct oxidation path prevails, H_2 being the main reaction product, with no HDO formation (see Fig. 6).

4. Conclusions

The rate results obtained in the vapor-phase photocatalytic methanol reforming on noble metal-modified TiO_2 at different methanol molar fractions adequately fit a reaction scheme implying three parallel oxidation paths: (i) an indirect ·OH-radical-mediated path; (ii) a direct path, implying the reaction of valence band holes with adsorbed methanol at the titania–noble metal interface; and (iii) a water-assisted direct path, involving the reaction of valence band holes with methanol molecules adsorbed far from the titania–noble metal interface. In this case, water plays a double role: (a) as an oxygen donor in the formaldehyde to formic acid oxidation step and (b) as a proton diffusion medium from surface oxidation sites to noble metal nanoparticles. The relative importance of the indirect oxidation path, very selective toward CO_2 production and occurring on relatively strong adsorption sites of the photocatalyst surface under irradiation, rapidly decreases with increasing the methanol molar fraction in the feed, prevailing only for x < 0.1. The proposed mechanism is fully supported by H_2O/D_2O isotopic exchange experiments.

Acknowledgments

The authors are very grateful to Prof. Lucio Forni for fruitful discussion. Financial support from the Cariplo Foundation through the Project *Visible Light Sensitive Photocatalytic Materials for Separate Hydrogen Production Devices* is gratefully acknowledged.

References

[1] A. Kudo, Y. Miseki, Chem. Soc. Rev. 38 (2009) 253.
[2] G.L. Chiarello, E. Selli, Recent Pat. Eng. 4 (2010) 155.
[3] M. Kitano, M. Hara, J. Mater. Chem. 20 (2010) 627.
[4] P.V. Kamat, J. Phys. Chem. B 106 (2002) 7729.
[5] G.L. Chiarello, M.H. Aguirre, E. Selli, J. Catal. 273 (2010) 182.
[6] A. Yamakata, T. Ishibashi, H. Onishi, J. Phys. Chem. B 107 (2003) 9820.
[7] J. Chen, D.F. Ollis, W.H. Rulkens, H. Bruning, Water Res. 33 (1999) 669.
[8] D.W. Bahnemann, M. Hilgendorff, R. Memming, J. Phys. Chem. B 101 (1997) 4265.
[9] T. Lana Villarreal, R. Gomez, M. Neumann-Spallart, N. Alonso-Vante, P. Salvador, J. Phys. Chem. B 108 (2004) 15172.
[10] C.S. Turchi, D.F. Ollis, J. Catal. 122 (1990) 178.
[11] C.Y. Wang, R. Pagel, D.W. Bahnemann, J.K. Dohrmann, J. Phys. Chem. B 108 (2004) 14082.
[12] J.M. Kesselman, O. Weres, N.S. Lewis, M.R. Hoffmann, J. Phys. Chem. B 101 (1997) 2637.
[13] C. Minero, G. Mariella, V. Maurino, E. Pelizzetti, Langmuir 16 (2000) 2632.
[14] S. Yamazaki, S. Tanaka, H. Tsukamoto, J. Photochem. Photobiol. A 121 (1999) 55.
[15] D.F. Ollis, J. Phys. Chem. B 109 (2005) 2439.
[16] G. Wu, T. Chen, W. Su, G. Zhou, X. Zong, Z. Lei, C. Li, Int. J. Hydrogen Energy 33 (2008) 1243.
[17] A. Gora, B. Toepfer, V. Puddu, G. Li Puma, Appl. Catal. B: Environ. 65 (2006) 1.
[18] B. Toepfer, A. Gora, G. Li Puma, Appl. Catal. B: Environ. 68 (2006) 171.
[19] C.S. Turchi, D.F. Ollis, J. Catal. 119 (1989) 483.
[20] M.R. Hoffmann, S.T. Martin, W. Choi, D.W. Bahnemann, Chem. Rev. 95 (1995) 69.
[21] G.L. Chiarello, I. Rossetti, L. Forni, J. Catal. 236 (2005) 251.
[22] J.H. Liu, A.Q. Wang, Y.S. Chi, H.P. Lin, C.Y. Mou, J. Phys. Chem. B 109 (2005) 40.
[23] G.L. Chiarello, L. Forni, E. Selli, Catal. Today 144 (2009) 69.
[24] G.L. Chiarello, E. Selli, L. Forni, Appl. Catal. B: Environ. 84 (2008) 332.
[25] A. Fujishima, X. Zhang, D.A. Tryk, Surf. Sci. Rep. 63 (2008) 515.
[26] E.A. Taylor, G.L. Griffin, J. Phys. Chem. 92 (1988) 471.
[27] W. Wu, C. Chuang, J. Lin, J. Phys. Chem. B 104 (2000) 8719.
[28] A. Yamakata, T. Ishibashi, H. Onishi, J. Phys. Chem. B 106 (2002) 9122.
[29] C. Wang, H. Groenzin, M.J. Shultz, J. Phys. Chem. B 108 (2004) 265.
[30] T. Chen, Z. Feng, G. Wu, J. Shi, G. Ma, P. Ying, C. Li, J. Phys. Chem. C 111 (2007) 8005.
[31] S.P. Bates, M.J. Gillan, G. Kresse, J. Phys. Chem. B 102 (1998) 2017.
[32] A. Tilocca, A. Selloni, J. Phys. Chem. B 108 (2004) 19314.

[33] Y. Han, C. Liu, Q. Ge, J. Phys. Chem. C 113 (2009) 20674.
[34] S. Wendt, J. Matthiesen, R. Schaub, E.K. Vestergaard, E. Lægsgaard, F. Besenbache, B. Hammer, Phys. Rev. Lett. 96 (2006) 066107.
[35] R.C. Reid, J.M. Prausnitz, B.E. Poling, The Properties of Gases & Liquids, fourth ed., McGraw-Hill, New York, 1987. p. 254.
[36] S. Yurdakal, G. Palmisano, V. Loddo, V. Augugliaro, L. Palmisano, J. Am. Chem. Soc. 130 (2008) 1568.
[37] V. Augugliaro, H. Kisch, V. Loddo, M.J. Lopez-Munoz, C. Marquez-Alvarez, G. Palmisano, L. Palmisano, F. Parrino, S. Yurdakal, Appl. Catal. A: General 349 (2008) 182.